A Robust Self Triggered Image Based Visual Servoing Model Predictive Control Scheme for Small Autonomous Robots

Shahab Heshmati-alamdari, George C. Karras, Alina Eqtami and Kostas J. Kyriakopoulos

***Abstract*— It is well known that a real-time visual servoing task which employs a Visual Tracking Algorithm (VTA) imposes high computational cost to robotic system, which consequently results in higher energy consumption and lower autonomy. Motivated by this fact, this paper presents a novel Image Based Visual Servoing-Model Predictive Control (IBVS-MPC) scheme which is combined with a mechanism that decides when the VTA needs to be triggered and new control inputs must be calculated. Between two consecutive triggering instants, the control input trajectory is applied to the robot in an open-loop fashion, i.e, no visual measurements and calculation of the control inputs are required during that period. This results in the reduction of the computational effort, energy consumption and increases the autonomy of the system. These factors are of utmost importance in the case of small autonomous robotic systems which perform vision based tasks, such as surveillance and inspection of indoors and outdoors environments. The visibility and inputs constraints, optimality rate of the MPC, as well as the external disturbances, are being considered during the control design. The efficiency of the proposed scheme is demonstrated through a set of real-time experiments using an eye-in-hand mobile robotic system.**

I. Introduction

Visual Servoing consists in using the camera as a sensor for the communication of the robot with the environment, and using the visual feedback for the determination of the control input. Structurally, it can be classified as: (i) Position-Based Visual Servoing (PBVS), (ii) Image-Based Visual Servoing (IBVS) and (iii) 2-1/2 Visual Servoing where the $3D$ PBVS is combined with $2D$ IBVS [1], [2].

In this work, the IBVS scheme is considered, as it is more efficient than the other two, owing to its inherent robustness against camera calibration imperfections. A significant issue in visual servoing is handling the visibility constraints, imposed by the fact that the image features are required not to leave the Field Of View (FOV) of the camera during its motion [3]. In order to handle the visibility constraints various methods have been developed. More specifically, in [4] and [5] path planning of the image features based on the motion of the camera in 3D space are presented. Moreover in [6] a novel strategy based on the prescribed transient and steady state response on the image feature error is presented.

Nonlinear Model Predictive Control (NMPC) [7], due to its strong and efficient ability to handle input and state constraints is an ideal approach to be used in IBVS. The IBVS-NMPC framework has been studied in [8], [9], [10] and [11]. In our previous work [8] a robustness analysis of the IBVS-MPC with respect to (w.r.t) the disturbances and noises on the image features has been proposed. The Visual Predictive Control (VPC) scheme has been proposed in [9] where the visibility constraints are formulated as state constraints. Some applications of IBVS-MPC for navigation of an Unmanned Aerial Vehicles (UAV), as well as some medical applications have been presented in [10] and in [11], respectively.

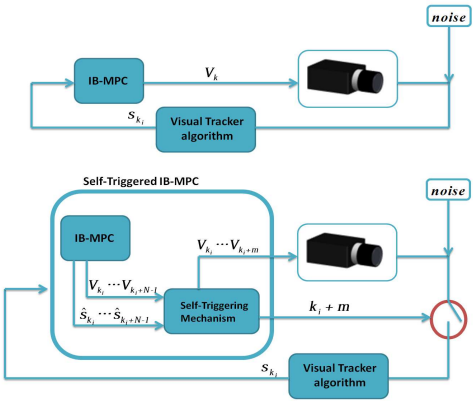

Fig. 1: The classic IBVS-MPC and ST-IBVS-MPC are depicted in the top and bottom diagrams respectively.

A standard visual servoing scheme consists the periodic use of the vision feedback which is extracted from the image to generate a task error and using a control algorithm to minimize this error. The process of image feature extraction, matching with a desired image and using them to generate the task error, is usually referred in the literature as the *Visual Tracking* [12]. It is well known that, a real-time robotic application in a complex environment, the accurate and robust Visual Tracking Algorithm (VTA) is very heavy process and has high computational cost which usually results in large energy usage and delays on the closed loop system.

This problem becomes more apparent when small autonomous robotic systems are considered such as Autonomous Underwater Vehicles (AUVs) and UAVs that suffer from limited energy resources (batteries) and usually are equipped with small and not so powerful embedded computing unit. Long lasting inspection tasks in complex environments require accurate VTA and concurrently high autonomy rate of the system. The problem then, becomes more evident, because the continuous recharging procedure is undesirable, difficult and time consuming. In addition, the continuous

Shahab Heshmati-alamdari, George C. Karras and Kostas J. Kyriakopoulos are with the Control Systems Lab, Department of Mechanical Engineering, National Technical University of Athens, 9 Heroon Polytechniou Street, Zografou 15780, Greece{shahab,karrasg,kkyria@mail.ntua.gr}.
Alina Eqtami is with Cardiovascular Surgery, Childrens Hospital Boston, Harvard Medical School, Boston MA, 02115, USA. {alina.eqtami@childrens.harvard.edu}.

visual tracking at every sampling time owing to the existence of a weak computing unit in these systems, leads to bigger sampling periods on the closed loop system, that consequently reduce the accuracy of the system.

Now, is it possible to design a visual servoing scheme that decides when the robot needs to track the visual information and when not, while the whole system does not lose the required performance? This question, motivates the self-triggered design framework for Visual Servoing in order to track the vision information and compute the control law only when it is needed. Generally, in Self Triggered control the key attribute is that the decision for sampling the state measurement as well as the execution of the control task is not made ad-hoc as in the sampled-data case, but it takes into account state or output feedback, see Fig1. Some introductory papers on self-triggered control can be found in [13] and [14]. In our previous work [15] a Self Triggered Position Based Visual Servoing scheme for an under-actuated underwater robotic vehicle was given. In this work we extend our previous work into a general image based version by presenting the Robust Self Triggered-Image Based Visual Servoing-Model Predictive Control (ST-IBVS-MPC) scheme. The mechanism of the proposed framework, decides when the next VTA should occur. This results to the reduction of the computational effort, processing of vision data, energy consumption and therefore it increases the autonomy rate of the system. The visibility and inputs constraints, optimality rate, as well as the external disturbances, are also being considered during the control design.

The paper is organized as follows: Modeling of the IBVS is given in Section II. Section III includes the problem statement and the control design. Section IV accommodates the stability analysis of the proposed self-triggered IBVS-MPC scheme. In Section V a comparative experimental study is given and finally, Section VI concludes the paper.

II. Mathematical Modelling

Let $[X_c, Y_c, Z_c]^\top$ be the axes of the camera frame $\mathcal{C}$ attached at the center of the camera O_c. The coordinates of the image frame $\mathcal{I}$ are given by $[u, v]^\top$ with O_I denoting the center of the image, as depicted in Fig. 2. Given a set of

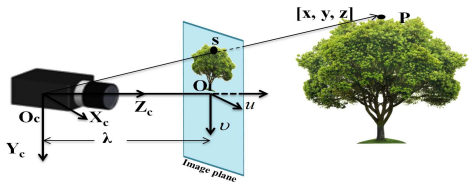

Fig. 2: The coordinate frame of the camera system.

n fixed 3D points $P^i = [x^i, y^i, z^i]^\top$, $i = 1, \dots, n$ expressed in the camera frame, the corresponding 2D image feature $s^i = [u^i, v^i]^\top$, $i = 1, \dots, n$ are given as follows [12]:

$$s^i = \begin{bmatrix} u^i \\ v^i \end{bmatrix} = \frac{\lambda}{z^i} \begin{bmatrix} x^i \\ y^i \end{bmatrix} \tag{1}$$

where λ is the focal length of the camera (see Fig.2). The time derivative of (1) is given by:

$$\dot{s}^i = L^i(z^i, s^i)V,\ i = 1, \dots, n \tag{2}$$

where: $L^i\left(z^i, s^i\right) =$

$$= \begin{bmatrix} -\frac{\lambda}{z^i} & 0 & \frac{u^i}{z^i} & \frac{u^i v^i}{\lambda} & -\frac{(\lambda^2+(u^i)^2)}{\lambda} & v^i \\ 0 & -\frac{\lambda}{z^i} & \frac{v^i}{z^i} & \frac{(\lambda^2+(v^i)^2)}{\lambda} & -\frac{u^i v^i}{\lambda} & -u^i \end{bmatrix}$$

is the interaction matrix [12], and $V = [T, \Omega]^\top = [T_x, T_y, T_z, \omega_x, \omega_y, \omega_z]^\top$, denotes the translational and angular velocities of the camera which represents the control input of the system. Let us also define the overall image feature vector $s = \left[{s^i}^\top, \cdots, {s^i}^\top\right]^\top \in \mathbb{R}^{2n}$, the time derivative of which is given by:

$$\dot{s} = L(z, s)V \tag{3}$$

where $L(z, s) = \left[{L^i}^\top\left(z^i, s^i\right), \cdots, {L^n}^\top\left(z^n, s^n\right)\right]^\top$ is the overall interaction matrix and $z = \left[z^i, \dots, z^n\right]^\top$. Using the Newton-Euler method for approximating (3), the model of the system in the discrete-time frame becomes:

$$s_{k+1} = s_k + dt(\widehat{L}_k \cdot V_k) \tag{4}$$

where dt and k are the sampling period and time-step respectively. It is obvious that the $\widehat{L}_k$ depends on depth parameter, thus two cases one with *unknown* and one with *known* depth parameter can be considered. In the first one, the depth parameter is unknown and it is replaced by its desired value in the desired position of the camera $z^i = z^{i^*}$, $i = 1 \dots n$. Although, in the *known* case, the depth parameter is available in each sampling time. For the rest of paper we denote $s_k = [{s_k^1}^\top, \cdots, {s_k^n}^\top]^\top$ to be the vector of the state at a time-step k. The vector of the velocity of the camera $V_k = [T_{(x,k)} \quad T_{(y,k)} \quad T_{(z,k)} \quad \omega_{(x,k)} \quad \omega_{(y,k)} \quad \omega_{(z,k)}]^\top$ will denote the input of the system at a time-step k. The aforementioned discrete-time system (4) is the nominal system and can be written in stack vector form as:

$$s_{k+1} = f(s_k, V_k) \tag{5}$$

The control constraint set V_{set} is compact and is given by:

$$V_k \in V_{set} \subseteq \mathbb{R}^6 \tag{6}$$

The constraints of the input are of the form $|T_x| \leq \bar{T}_x$, $|T_y| \leq \bar{T}_y$, $|T_z| \leq \bar{T}_z$, $|\omega_x| \leq \bar{\omega}_x$, $|\omega_y| \leq \bar{\omega}_y$ and $|\omega_z| \leq \bar{\omega}_z$. where $(\bar{\cdot})$ denotes the upper bound for each of the variables. We set $\|V_k\| \leq \bar{V}$, with $\bar{V}$ to be the upper bound for the control input of the system. Finally, owing to the limited field of view of the camera, the image coordinates are subject to the following visibility constraints:

$$u_{\min} \leq u^i \leq u_{\max},\ i = 1, \dots, n \tag{7a}$$

$$v_{\min} \leq v^i \leq v_{\max},\ i = 1, \dots, n \tag{7b}$$

where $u_{\min}$, $v_{\min}$ and $u_{\max}$, $v_{\max}$ are the lower and upper bounds (in pixels) of the image plane coordinates u, v respectively. These visibility constraints form the state constraint set $S_{set} \subseteq \mathbb{R}^{2n}$ i.e., $s_k \in S_{set}$. Assume that the system (5)

is affected by noise, in the form of output noise from the vision tracking algorithm. This noise is introduced into the system as an external disturbance vector that is formed by:

$$\xi_k = [{\xi_k^1}^\top \dots {\xi_k^n}^\top]^\top$$

where $\xi_k^i = [\xi_u^i, \xi_v^i]^\top \quad i = 1, \dots, n$. These disturbances form the compact disturbance set $\Xi \subseteq \mathbb{R}^{2n}$ with $\xi_k \in \Xi$, upper bounded by $\bar{\xi}$, where $||\xi_k|| \leq \bar{\xi}$, $\forall \xi_k \in \Xi$. Therefore, an actual system can be considered as:

$$s_{k+1} = f(s_k, V_k) + \xi_k \tag{8}$$

III. Control Design and Problem Statement

The goal is to control the actual system (8) subject to the visibility and control constraints of (7a)-(7b) and (6) to reach to a compact image feature set that includes the desired state $s_d = [s_d^1, \dots, s_d^n]^\top \in S_{set}$. In order to achieve this task we use a nonlinear model predictive controller that consists in solving iteratively an open-loop Optimal Control Problem (OCP) w.r.t a control sequence $V_f(k)$. The OCP of the IBVS-MPC is given as follows:

$$\min_{V_f(k)} J_N(s_k, V_f(k)) = \tag{9a}$$

$$\min_{V_f(k)} \sum_{i=0}^{N-1} F(\hat{s}(k+i|k), V(k+i|k)) + E(\hat{s}(k+N|k))$$

subject to

$$\hat{s}(k+j|k) \in S_j, \qquad \forall j = 1, \dots, N-1, \tag{9b}$$

$$V(k+j|k) \in V_{set}, \qquad \forall j = 0, \dots, N-1, \tag{9c}$$

$$\hat{s}(k+N|k) \in \mathscr{E}_f \tag{9d}$$

where N denotes the prediction horizon and the set $\mathscr{E}_f$ is the terminal set. F and E are the running and terminal cost functions, respectively and are of quadratic form, i.e., $F(\hat{s}, V) = \hat{s}^\top Q \hat{s} + V^\top R V$ and $E(\hat{s}) = \hat{s}^\top P \hat{s}$, with P, Q and R to be positive definite matrices. Particularly we define $Q = diag\{q_1, q_2, \cdots, q_{(2n-1)}, q_{(2n)}\}$, $R = diag\{r_1, r_2, r_3, r_4, r_5, r_6\}$ and $P = diag\{p_1, p_2, \cdots, p_{(2n-1)}, p_{(2n)}\}$. The vector $\hat{s}(k+j|k)$ denotes the predicted state of the nominal system (5) at sampling time $k+j$ with $j \in \mathbb{Z}_{\geq 0}$. The predicted state is based on the measurement of the image features s_k at a sampling time k, while applying a sequence of control inputs $\{V_k, \dots, V_{k+j-1}\}$. Thus: $\hat{s}(k+j|k) = f(\hat{s}(k+j-1|k), V_{k+j-1})$. It holds that $\hat{s}(k|k) = s_k$. We distinguish the state of nominal system that will be denoted as $\hat{s}(\cdot)$ with the state of actual system, i.e. the system that is affected by disturbances which will be denoted as $s(\cdot)$.

Lemma 1 [8]: The nominal system (5), subject to constraints (7a)-(7b) and (6), is Lipschitz continuous in S_{set} with Lipschitz constant $0 < C_f < \infty$. More specifically in the case of *unknown* depth parameter can be defined as:

$$C_f \triangleq 5\sqrt{2}\max\left\{(\frac{dt\bar{T}_z}{z^{i^*}}), (\frac{2\sqrt{2}\bar{\omega}_x dt\max(\bar{u},\bar{v})}{\lambda}), (\frac{2dt\bar{\omega}_x\bar{v}}{\lambda}), (dt\bar{\omega}_z), (\frac{2dt\bar{\omega}_y\bar{u}}{\lambda}), (\frac{2\sqrt{2}\bar{\omega}_y dt\max(\bar{u},\bar{v})}{\lambda}), 1\right\} \tag{10}$$

And, when the depth parameter is *known*, it is given by:

$$C_f \triangleq 5\sqrt{2}\max\left\{1, (\frac{dt\bar{T}_z\bar{u}}{z^*}), (\frac{2\sqrt{2}\bar{\omega}_x dt\max(\bar{u}\bar{v})}{\lambda}), (\frac{2dt\bar{\omega}_y\bar{u}}{\lambda}), , (\frac{2\sqrt{2}\bar{\omega}_y dt\max(\bar{u}\bar{v})}{\lambda}), (\frac{2dt\bar{\omega}_x\bar{v}}{\lambda}), (\frac{dt\lambda\bar{T}_x}{z^*}), (\frac{dt\lambda\bar{T}_y}{z^*}), (dt\bar{\omega}_z)\right\} \tag{11}$$

Lemma 2 [8]: The difference between the real state s_{k+j} at the time $k+j$ and the predicted state $\hat{s}(k+j|k)$ at the same time under the same control sequence, is upper bounded by:

$$||s_{k+j} - \hat{s}(k+j|k)|| \leq \sum_{i=0}^{j-1} (C_f)^i \bar{\xi} \tag{12}$$

Lemma 3 [8]: The cost function $F(s, V)$ is lower bounded by a $\mathcal{K}_\infty$-function. In particular:

$$F(s, V) \geq min(q_1, \cdots, q_{2n}, r_1, \cdots, r_6)||s||^2 \tag{13}$$

Lemma 4 [8]: The cost function $F(s, V)$ is Lipschitz continuous in $S_{set} \times V_{set}$, with Lipschitz constant C_F, where:

$$C_F = 2(n(\bar{u}^2 + \bar{v}^2))^{\frac{1}{2}} \cdot \sigma_{max}(Q) \tag{14}$$

where $\sigma_{max}(Q)$ denotes the largest singular value of the Q.

Assumption 1: There is an admissible positively invariant set $\mathscr{E} \subset S_{set}$ such that $\mathscr{E}_f \subset \mathscr{E}$, where $\mathscr{E} = \{s \in S_{set} : ||s|| \leq \varepsilon_0\}$ with ε_0 being a positive parameter.

Assumption 2: Inside the $\mathscr{E}_f$, there is a local controller $V_k = h(s_k) \in V_{set}, \quad \forall s \in \mathscr{E}$ and a Lyapunov function E such that $E(f(s_k, h(s_k))) - E(s_k) + F(s_k, h(s_k)) \leq 0$.

Assumption 3: The associated Lyapunov function for the terminal region is Lipschitz in $\mathscr{E}$, with Lipschitz constant $C_E = 2\varepsilon_0\sigma_{max}(P)$ for all $s \in \mathscr{E}$. Considering that from *Assumption 1* we have: $||s|| = (|u^1|^2 + |v^1|^2 + \cdots + |u^n|^2 + |v^n|^2)^{\frac{1}{2}} \leq \varepsilon_0$ for all $s \in \mathscr{E}$.

Assumption 4: Inside the set $\mathscr{E}$ we have $E(s) = s^T P s \leq \alpha_\varepsilon$, where $\alpha_\varepsilon = max\{p_1, \cdots, p_{(2n)}\}\varepsilon_0^2 > 0$. Assuming that $\mathscr{E} = \{s \in S_{set(N-1)} : h(s) \in V_{set}\}$ and taking a positive parameter α_{ε_f} such that $\alpha_{\varepsilon_f} \in (0, \alpha_\varepsilon)$, we assume that the terminal set $\mathscr{E}_f = \{s \in \mathbb{R}^3 : E(s) \leq \alpha_{\varepsilon_f}\}$ is such that $\forall s \in \mathscr{E}$, $f(s, h(s)) \in \mathscr{E}_f$.

A. Problem Statement

The solution of the Image based Model Predictive Controller (9a)-(9d) at a time-step k provides an control sequence V_f^* which equals to $V_f^*(k) \triangleq [V^*(k|k), \dots, V^*(k+N-1|k)]$. In the classic IBVS-MPC approach, only the first control vector, i.e $V^*(k|k)$ is applied to the system. At the next time-step $k+1$, the VTA is computed and new vision measurements are received and then the whole procedure is repeated again. In this paper, we suggest that a portion of the computed control sequence may be applied to the system and not only the first vector. More specifically, suppose a triggering instant k_i, at which the VTA has been computed and the IBVS-MPC has been solved. The control sequence that will now be applied to the robot is of the form:

$$[V^*(k_i|k_i), V^*(k_i+1|k_i), \dots V^*(k_i+d_i|k_i)] \tag{15}$$

for all $d_i \in [1, k_{i+1} - k_i] \in \mathbb{Z}_{\geqslant 1}$, where k_{i+1} is the next triggering instant. During the time interval $[k_i, k_{i+1})$ the control law is applied to the robot in an open-loop fashion. But how large this time interval can be? This paper, addresses this question and provides sufficient conditions for finding the triggering periods d_i, or in other words sufficient conditions for running the VTA and the computation of the NMPC law.

IV. Stability Analysis of Self-triggering IBVS-MPC framework

We begin the stability analysis by assuming that at $k_i \triangleq k-1$ an event is triggered, the solution of the (9a)-(9d) at this time results in an optimal control trajectory $V_f^*(k-1) \triangleq [V^*(k-1|k-1), \ldots, V^*(k+N-2|k-1)]$. Based on this optimal control trajectory, we can define a feasible control input, i.e., for $m = 0, \ldots, N-2$ given by:

$$\tilde{V}(k+j|k+m) = \begin{cases} V^*(k+j|k-1) & \text{for} \quad j = m, \ldots, N-2 \\ h(\hat{s}(k+j|k+m)) & \text{for} \quad j = N-1, \ldots, N+m-1 \end{cases} \tag{16}$$

From the (9c) and with the help of Assumption 2, it follows that for $m = 0, \ldots N-2$ we have $\tilde{V}(k+j|k+m) \in V_{set}$. The stability analysis consists of two parts: (i) feasibility property and (ii) Convergence property.

A. Feasibility of ST-IBVS-MPC

Let $\mathcal{S}^{IB}$ be the set containing all the state vectors for which a feasible control sequence exists that satisfies the constraints of the optimal control problem. Now we are going to find an upper bound $\bar{\xi}$ for disturbances such that $\hat{s}(k+N|k+m) \in \mathscr{E}_f$ for all $m = 0, \ldots, N-2$.

Theorem 1: Consider the IBVS system (8) that is subject to constraints (7a)(7b) and (6). Assume that at $k_i \triangleq k-1$ an event is triggered, thus the VTA is activated, the OCP of (9a)-(9d) is solved and a new control sequence is provided. A partition of this control sequence, for $m \in [0, \ldots, N-2]$ drives and stabilizes the image features vector s to a set $\mathscr{E}$ around the desired image features vector s^*, satisfying all constraints, if and only if the disturbances are bounded by:

$$\bar{\xi} \leq \frac{\alpha_\varepsilon - \alpha_{\varepsilon_f}}{C_E C_f^{(N-1)-m} \sum_{i=0}^{m} (C_f^i)} \tag{17}$$

Proof: From Lemma 2 we can derive the following:

$$\begin{aligned} &||\hat{s}(k+N-1|k+m) - \hat{s}(k+N-1|k-1)|| \leq \\ &\leq C_f^{(N-1)-m} \sum_{i=0}^{m} (C_f^i) \bar{\xi} \end{aligned}$$

From the Lipschitz property of $E(\cdot)$ (*Assumption* 3) we get:

$$\begin{aligned} &E(\hat{s}(k+N-1|k+m)) - E(\hat{s}(k+N-1|k-1)) \\ &\leq C_E ||\hat{s}(k+N-1|k+m) - \hat{s}(k+N-1|k-1)|| \\ &\leq C_E C_f^{(N-1)-m} \sum_{i=0}^{m} (C_f^i) \bar{\xi} \end{aligned}$$

Noticing that $\hat{s}(k+N-1|k-1) \in \mathscr{E}_f$, from *Assumption* 4 we get $E(\hat{s}(k+N-1|k-1)) \leq \alpha_{\varepsilon_f}$. We want $\hat{s}(k+N-1|k+m) \in \mathscr{E}$, thus from *Assumption* 4, it should satisfy $E(\hat{s}(k+N-1|k+m) \leq \alpha_\varepsilon$, so we get:

$$E(\hat{s}(k+N-1|k+m) \leq \alpha_{\varepsilon_f} + C_E q(m) \bar{\xi} \leq \alpha_\varepsilon$$

with $q(m) \triangleq C_f^{(N-1)-m} \sum_{i=0}^{m} (C_f^i)$. Thus, we obtain:

$$\alpha_{\varepsilon_f} + C_E q(m) \bar{\xi} \leq \alpha_\varepsilon \Rightarrow \bar{\xi} \leq \frac{\alpha_\varepsilon - \alpha_{\varepsilon_f}}{C_E C_f^{(N-1)-m} \sum_{i=0}^{m} (C_f^i)} \tag{15}$$

which states that the set $\mathcal{S}^{IB}$ is robustly positively invariant for disturbances bounded by (15) for all $m = 0, \ldots, N-2$, and from from *Assumption* 4 we get $\hat{s}(k+N|k+m) \in \mathscr{E}_f$, which concludes the proof. ■

B. Convergence of ST-IBVS-MPC

At the time-step $k-1$, the optimal cost is denoted as $J_N^*(k-1) = J_N(s_{k-1}, V_f^*(k-1))$, which is evaluated under the optimal control sequence. Analogously, the optimal cost at a time-step $k+m$ with $m \in [0, N-2]$ is denoted as $J_N^*(k+m) = J^*(s_{k+m}, V_f^*(k+m))$. Now let $\tilde{J}_N(k+m)$ to denote the "feasible"cost, evaluated from the control sequence $\tilde{V}_f^m(k-1)$, that is $\tilde{J}_N(k+m) = \tilde{J}_N(s_{k+m}, \tilde{V}_f^m(k-1))$. It is well known that in a real experiment with a real robotic system, owing to the finite iteration's number of the optimization procedure, it is not possible to find the exact optimal solution of (9a)-(9d) and always some sub-optimality rate must be considered. Thus for the feasible cost function defined above we consider a "real"version of it denoted by $\tilde{J}'(\cdot)$ and a sub-optimality rate denoted by B such that $B = \frac{\tilde{J}}{\tilde{J}'}, B \in (0, 1]$. Now, the difference between the real-feasible sequence at time-step $k+j$ and the optimal cost at time $k-1$ using (16) is given by:

$$\begin{aligned} &\Delta J_m = \tilde{J}'_N(k+m) - J^*{}_N(k-1) = \\ &= \tilde{J}_N(k+m) - J_N^*(k-1) + \tilde{J}_N(k+m)(\frac{1}{B} - 1) \leq \\ &\leq C_E (C_f)^{(N-(m+1))} \bar{\xi} + L_S(m) - \\ &- L_Q(m) + (\frac{1}{B} - 1)\big(L_S(m) + L_P(m) + \max(p_1, \ldots, p_{2n}) \varepsilon_0^2\big) \end{aligned} \tag{16}$$

Where:

$$L_S(m) = C_F \cdot \sum_{i=0}^{N-(m+2)} (C_f)^i \bar{\xi},$$

$$L_P(m) = \max(p_1, \ldots, p_{2n}, r_1, \ldots, r_6) \sum_{i=0}^{N-(m+2)} ||[\hat{s}(\cdot), V^*(\cdot)]||$$

and

$$L_Q(m) = \sum_{i=-1}^{m-1} min(q_1, \ldots, q_{(2n)} r_1, \ldots, r_6) ||\hat{s}(k+i|k-1)||$$

where we denote by $:(\cdot) = (k+i+m|k-1)$. The optimality of the solution yields:

$$J^*{}_N(k+m) - J^*{}_N(k-1) \leq \tilde{J}'_N(k+m) - J^*{}_N(k-1) \tag{17}$$

C. The Self-triggered Framework

Consider that at time-step k_i a measurement from VTA is received and a new control input is calculated. The next triggering time $k_{i+1} \triangleq k_i + d_i$ that is going to be found

should be such that the closed-loop system of IBVS-MPC does not loose any of its desired performances. Thus, we need the value function $J_N^*(\cdot)$ to be decreasing. Given (16) and (17), for some triggering instant k_i and some time-step $d_i = m+1$ with $d_i \in [1, N-1]$ we get:

$$J_N^*(k_{i+1}) - J_N^*(k_i) \leq C_E(C_f)^{(N-(d_i))}\bar{\xi} + L_S - \\ - L_Q + (\frac{1}{B} - 1)\big(L_S + L_P + \max(p_1, \ldots, p_{2n})\varepsilon_0^2\big) \quad (18)$$

Thus, the time instance d_i should be such that:

$$\sigma L_Q \geq C_E(C_f)^{(N-(d_i))}\bar{\xi} + L_S(m) + \\ + (\frac{1}{B} - 1)\big(L_S(m) + L_P(m) + \max(p_1, \ldots, p_{2n})\varepsilon_0^2\big) \quad (19)$$

with $\sigma \in (0, 1)$. Plugging (19) and (18), it yields:

$$J_N^*(k_{i+1}) - J_N^*(k_i) \leq (\sigma - 1)L_Q(m) \quad (20)$$

In view of (20), it can be concluded that the Lyapunov function $J_N^*(\cdot)$ has been proven to be decreasing, thus the closed-loop system converges to the compact set $\mathscr{E}_f$. Thus, the next visual measurement needs to be triggered when (19) is violated. The condition (19) should be checked for each consecutive time-step, i.e., for $d_i = 1, 2, \ldots$. This time-step k_{i+1} also can be found beforehand at time k_i, because the term $L_Q(m)$ and $L_P(m)$ include only predictions of the nominal system. The pseudo-code of the proposed real-time self-triggering IBVS scheme is given in *Algorithm1*: At time

Algorithm 1 Self Triggered IBVS-MPC algorithm:

1: **Triggering:** ▷ At triggering time k_i
2: $s(k_i) \leftarrow$ VTA ▷ Trigger the VTA, get $s(k_i)$
3: $V_f^*(k_i) \leftarrow$ OCP$(s(k_i))$ ▷ Run OCP of (9a)-(9d)
4: **Solve eq.**(19) **for** d_i ▷ Notice: $m = d_i - 1$
5: $k_{i+1} = k_i + d_i$ ▷ The next triggering time
6: **for** $i = 1 \rightarrow d_i$ **do**
7: Apply the $V^*(k_i + i|k_i)$ to the robot.
8: **goto** *Triggering*.

k_i the VTA is triggered, the OCP of (9a)-(9d) has run and the control trajectory $V_f^*(k_i)$ for $[k_i, k_i + N - 1]$ is provided. The solution of (19) will provide the next update time k_{i+1}. During the time interval $i \in [k_i, k_{i+1})$ the control trajectory $V^*(k_i + i|k_i)$ is applied to the system in an open-loop fashion. Next, at time k_{i+1}, the VTA is triggered again, a new control trajectory based on the current vision measurement $s(k_{i+1})$ is provided and the whole procedure is repeated again until the camera reaches to the desired position. Now, we state the result for the ST-IBVS-MPC framework:

Theorem 2: Consider the Image Based Visual Servo system (8) that is subject to constraints (7a)(7b) and (6). The triggering times d_i provided by (19) and the IBVS-MPC law provided by (9a)-(9d) which is applied to the system in an open-loop fashion during the inter-sampling periods, drive the closed-loop system towards the compact set $\mathscr{E}_f$, where it is ultimately bounded.

V. Experimental Results

To verify the efficiency of the proposed IBVS scheme, two experiments were performed using a YouBot mobile-manipulator system equipped with a USB camera as depicted in Fig.3.

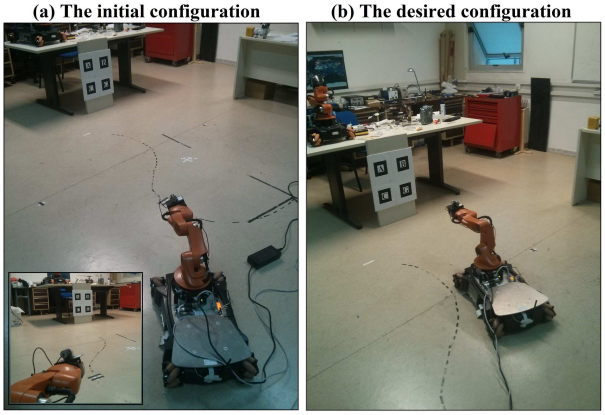

Fig. 3: The experimental setup (a) The initial and (b) The desired configuration.

A. Experimental Results

The comparison was performed via two experimental procedures. First, a conventional IBVS-MPC scheme was employed, while in the second experiment, the Self Triggered IBVS-MPC scheme proposed in this paper was employed. Comparisons are made to show the efficacy and performance of the proposed self triggered IBVS-MPC w.r.t the classic IBVS-MPC. The desired pose of the target wrt the camera frame in both experiments is $p^* = [0, 0, 0.6, -0.1, 0, 0]$. The desired features coordinates extracted by the desired image is given by: $s^* = [-61, -38, 60, -38, -56, 95, 62, 92]$. The initial configuration of the target w.r.t the camera and the initial feature coordinates in both experiments are given by: $p(0) = [1.74, 0.16, 2.81, 0.12, 0, -0.69]$ and $s(0) = [-68, -196, -25, -177 - 84, -136, -41, -122]$ respectively. It should be noticed that the above initial configuration, can be considered as a rather challenging task for IBVS schemes, owing to the rotation about the z and the x axes of the camera frame (see Fig.3). The visibility constraints of the system due the resolution of the image plane (640×480), are defined as:

$$\begin{bmatrix} \underline{u} = -319 \\ \underline{v} = -239 \end{bmatrix} \leq \begin{bmatrix} u(t) \\ v(t) \end{bmatrix} \leq \begin{bmatrix} \bar{u} = 319 \\ \bar{v} = 239 \end{bmatrix} \quad (21)$$

The prediction horizon and the sampling time in both experiments, are equal to $N = 6$ and $dt = 0.1$ respectively. The matrices P, Q and R of the OCP (9a)-(9d) are equal for both experiments. Also the control input is bounded by $0.5\frac{m}{sec}$ for the translational and $0.5\frac{rad}{sec}$ for rotational velocity. In Fig.4 the image error evolution in both experiments are depicted. It can be witnessed that in both cases, the image errors converge to zeros. As it was expected, the features were constrained within the camera FOV as presented in Fig. 5. In Fig.6, the triggering instants in the case of ST-IBVS-MPC are captured. When the vertical axis has the value 1, the VTA is triggered and a new image vector is calculated,

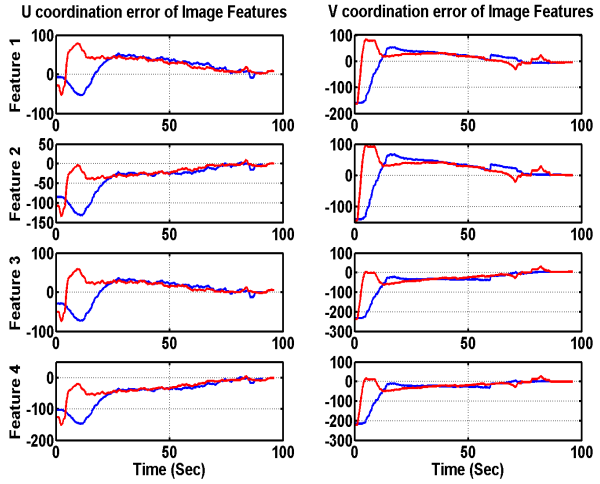

Fig. 4: The feature coordinate errors: the ST-IBVS-MPC and Classic IBVS-MPC are presented with blue and red color respectively.

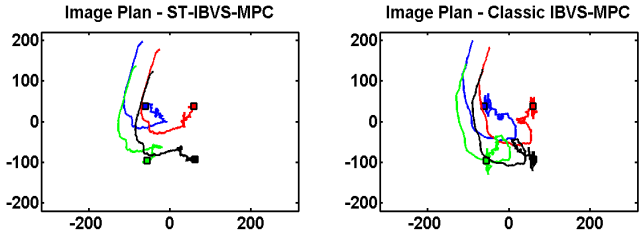

Fig. 5: The evolution of the features on the image plane. (a) ST-IBVS-MPC, (b) Classic IBVS-MPC.

consequently the IBVS-MP Controller is running and a new control input trajectory is computed. For value 0, the control law is implemented on the system in an open-loop fashion using the rest of the last computed control input trajectory. Notice that in the case of classic IBVS-MPC, the VTA is triggered at each sampling time. It can be noticed that the

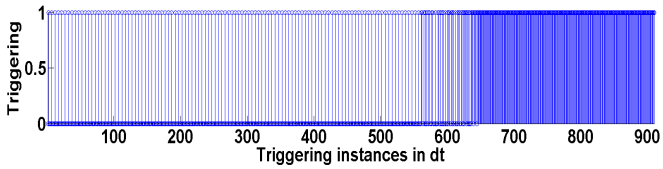

Fig. 6: The triggering instants for the case of ST-IBVS-MPC.

triggering instants when the camera is close to the desired position w.r.t the target are more frequent. This fact is easily interpretable, because near the desired position, the system becomes more demanding due to the F.O.V constraints and the disturbances, thus the need for new measurements and calculation of a new control input is increased. However, using the self triggered condition proposed in this work, the triggering of the VTA and the MPC controller have been reduced by 56% (405 triggering instants instead of 911) w.r.t the traditional IBVS-MPC.

VI. Conclusions

In this work a novel IBVS-MPC scheme is presented. A mechanism for the decision of the VTA triggering and the calculation of a new control input is designed and implemented. This results in the reduction of the computational effort, energy consumption and increases in this way the autonomy rate of the system. Thus it can be used effectively in small autonomous robotic systems which perform long lasting inspection tasks. Finally, future research efforts will be devoted towards experimental testing of the proposed control scheme on autonomous system with high external disturbances such as Underwater Vehicle-Manipulator System.

Acknowledgment

This work was supported by the "ROBOCADEMY", Marie Curie ITN Grant Agreement no FP7-608096 funded by the EU action "7^{th} Framework Programme - The 2013 People Work Programme - EC Call Identifier FP7-PEOPLE-2013-ITN, Implementation Mode: Multi-ITN"

References

[1] F. Chaumette and S. Hutchinson, "Visual servo control. i. basic approaches," *IEEE Robotics and Automation Magazine*, vol. 13, no. 4, pp. 82–90, 2006.

[2] F. Chaumette and S. Hutchinson, "Visual servo control, part ii: Advanced approaches," *IEEE Robotics and Automation Magazine*, vol. 14, no. 1, pp. 109–118, 2007.

[3] F. Chaumette, *Potential problems of stability and convergence in image-based and position-based visual servoing*. LNCIS Series, No 237, Springer-Verlag, 1998.

[4] M. Kazemi, K. Gupta, and M. Mehrandezh, "Global path planning for robust visual servoing in complex environments," *Proceedings of the 2009 IEEE International Conference on Robotics and Automation*, pp. 1726–1732, Kobe, Japan, 2009.

[5] Y. Mezouar and F. Chaumette, "Path planning for robust image-based control," *IEEE Transactions on Robotics and Automation*, vol. 18, no. 4, pp. 534–549, 2002.

[6] S. Heshmati-alamdari, C. P. Bechlioulis, M. V. Liarokapis, and K. J. Kyriakopoulos, "Prescribed performance image based visual servoing under field of view constraints," in *IEEE/RSJ International Conference on Intelligent Robots and Systems (IROS)*, September 2014.

[7] F. Allgwer, R. Findeisen, and Z. Nagy, "Nonlinear model predictive control: From theory to application," *the Chinese Institute of Chemical Engineers*, vol. 35, no. 3, pp. 299–315, 2004.

[8] S. Heshmati-alamdari, G. K. Karavas, A. Eqtami, M. Drossakis, and K. J. Kyriakopoulos, "Robustness analysis of model predictive control for constrained image-based visual servoing," *IEEE International Conference on Robotics and Automation*, 2014.

[9] G. Allibert, E. Courtial, and F. Chaumette, "Predictive control for constrained image-based visual servoing," *IEEE Transactions on Robotics*, vol. 26, no. 5, pp. 933–939, 2010.

[10] H. L. D. Lee and H. Kim, "Obstacle avoidance using image-based visual servoing integrated with nonlinear model predective control," *IEEE Conf. on Decision and Control and European Control Conference*, pp. 5689–5694, 2011.

[11] M. Sauve, P. Poignet, and E. Dombre, "Ultrasound image-based visual servoing of a surgical instrument through nonlinear model predictive control," *International Journal of Robotics Research*, vol. 27, no. 1, pp. 25–40, 2008.

[12] S. Hutchinson, G. Hager, and P. Corke, "A tutorial on visual servo control," *IEEE Transactions on Robotics and Automation*, vol. 12, no. 5, pp. 651–670, 1996.

[13] W. Heemels, K. Johansson, and P. Tabuada, "An introduction to event-triggered and self-triggered control," *IEEE 51st Conference on Decision and Control*, pp. 3270–3285, 2012.

[14] A. Anta and P. Tabuada, "To sample or not to sample: self-triggered control for nonlinear systems," *IEEE Transactions on Automatic Control*, vol. 55, no. 9, pp. 2030–2042, 2010.

[15] S. Heshmati-alamdari, A. Eqtami, G. C. Karras, D. V. Dimarogonas, and K. J. Kyriakopoulos, "A self-triggered visual servoing model predictive control scheme for under-actuated underwater robotic vehicles," *IEEE International Conference on Robotics and Automation*, 2014.